# On orbit calibration (for oceans and more)

Jeremy Werdell, Gene Eplee

PACE class @ UMBC
1-5 Aug 2022

GODDARD EARTH SCIENCES

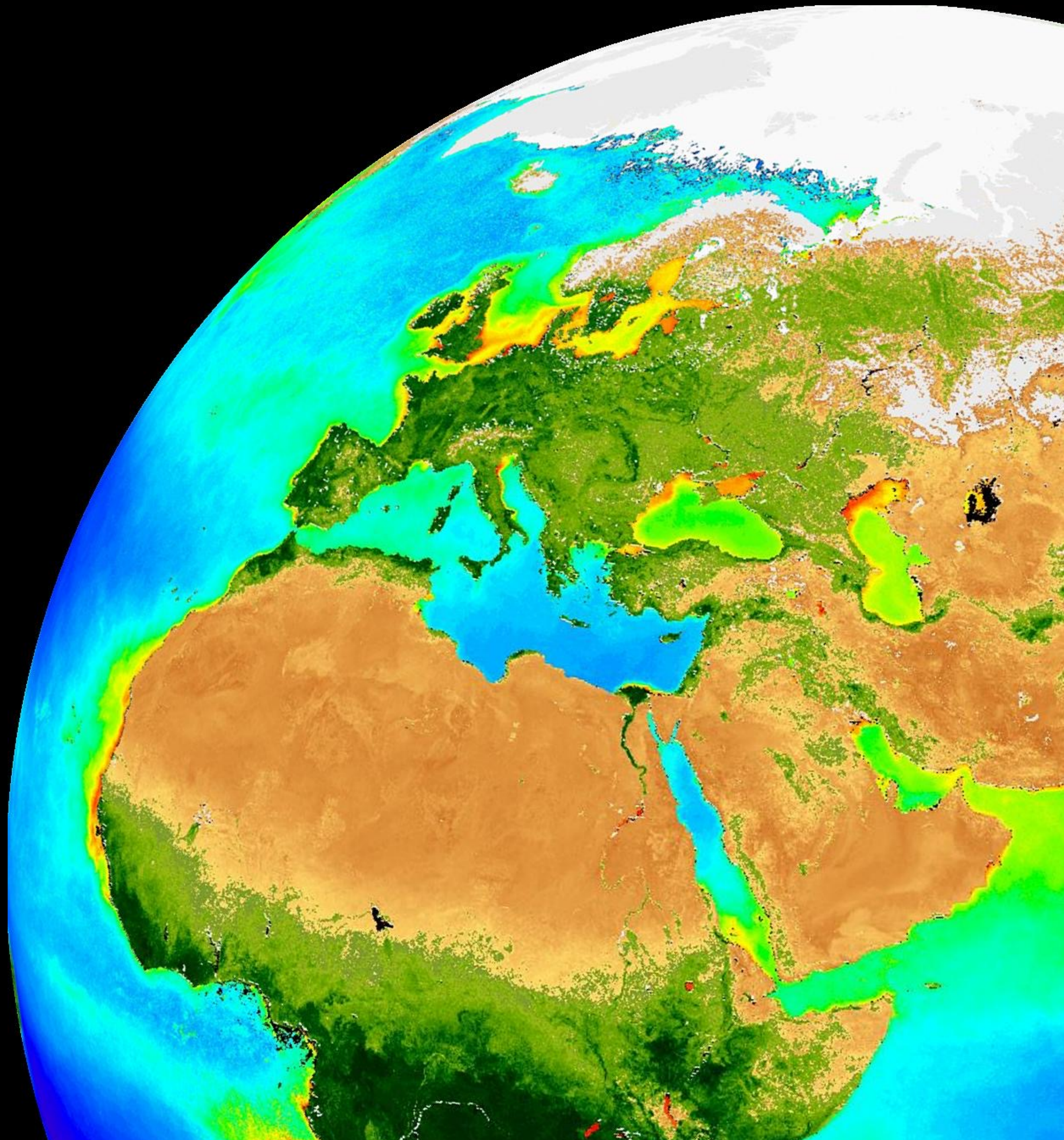

# post-launch calibrations

1. application and temporal assessment of pre-launch instrument calibrations
   - e.g., focal plane temperature

2. temporal calibration
   - reference Sun or Moon

3. absolute (system vicarious) calibration
   - reference Earth surface
   - final, single gain adjustment
   - calibration of the combined instrument + algorithm system

$$g_i = L_{t,i}^{target} / L_{t,i}^{satellite}$$

# sensors degrade on orbit

solar calibration

- evaluates short-term stability
- OCI has two (well, three) identical solar diffusors
  - one used daily
  - one used monthly (to verify performance of the daily diffusor)

lunar calibration

- evaluates long-term stability
- all NASA ocean color instruments apply lunar calibrations

# lunar calibration

relative calibration with $t_0$ = first observation

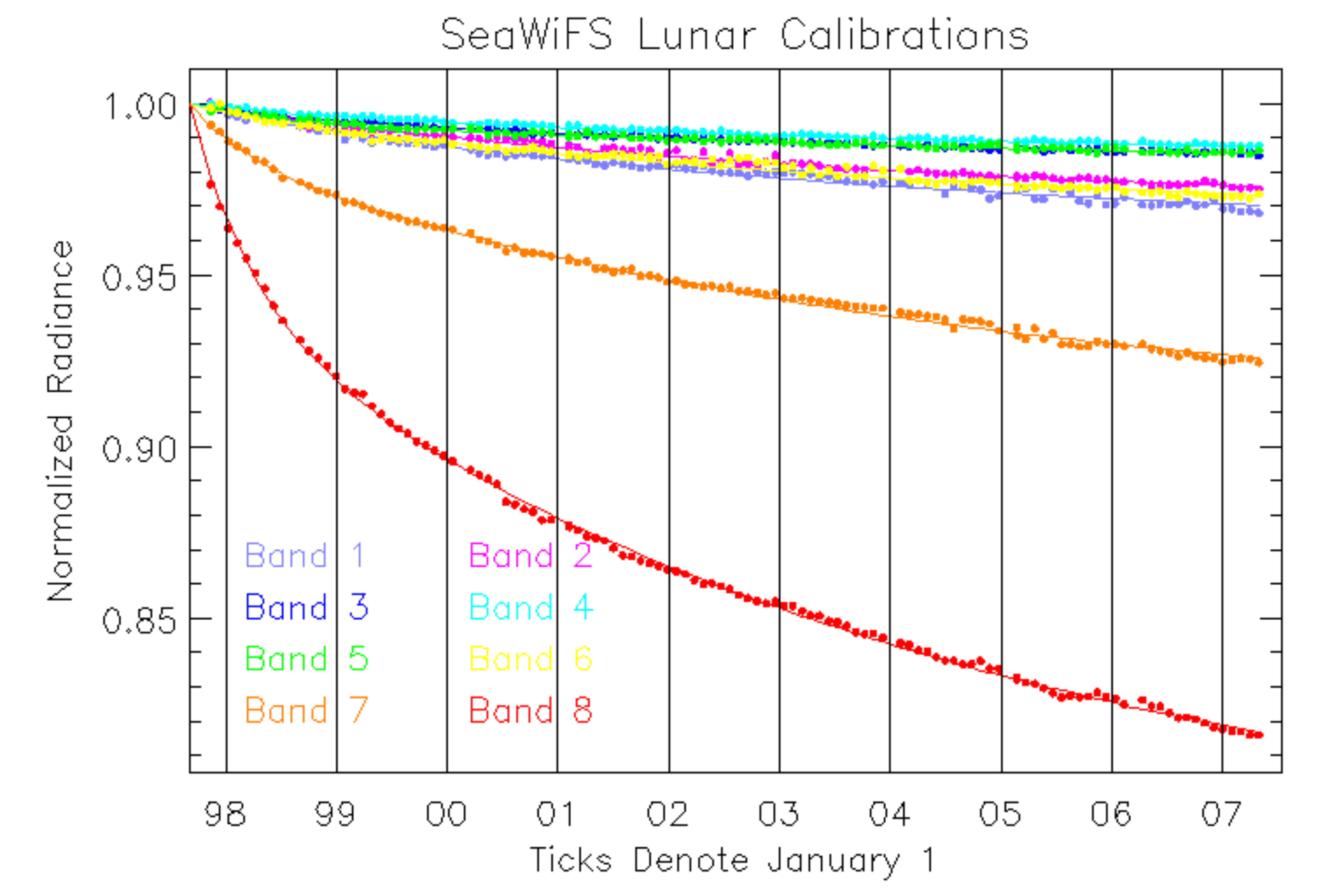

# the moon as a reference

USGS ROLO model
"Robotic Lunar Observatory"

THE ASTRONOMICAL JOURNAL, 129:2887–2901, 2005 June


THE SPECTRAL IRRADIANCE OF THE MOON

HUGH H. KIEFFER[1,2] AND THOMAS C. STONE
US Geological Survey, 2255 North Gemini Drive, Flagstaff, AZ 86001
*Received 2004 September 24; accepted 2005 March 5*

*remote sensing* MDPI

*Article*

**The Moon as a Climate-Quality Radiometric Calibration Reference**

**Thomas C. Stone [1,*], Hugh Kieffer [2], Constantine Lukashin [3] and Kevin Turpie [4]**

## Absolute Irradiance of the Moon for On-orbit Calibration

Thomas C. Stone and Hugh H. Kieffer
US Geological Survey, 2255 N. Gemini Dr., Flagstaff, AZ 86001, USA

**ABSTRACT**

The recognized need for on-orbit calibration of remote sensing imaging instruments drives the ROLO project effort to characterize the Moon for use as an absolute radiance source. For over 5 years the ground-based ROLO telescopes have acquired spatially-resolved lunar images in 23 VNIR (Moon diameter ~500 pixels) and 9 SWIR (~250 pixels) passbands at phase angles within ±90 degrees. A numerical model for lunar irradiance has been developed which fits hundreds of ROLO images in each band, corrected for atmospheric extinction and calibrated to absolute radiance, then integrated to irradiance. The band-coupled extinction algorithm uses

# lunar maneuvers

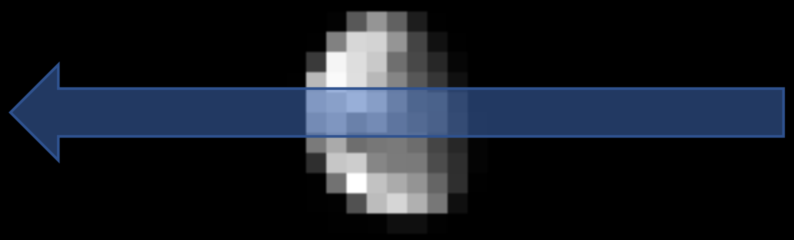


Chapter 9

Analysis of a Pushbroom Ocean Color Instrument Lunar Calibration

Frederick S. Patt, Science Applications International Corporation, Reston, Virginia[8]

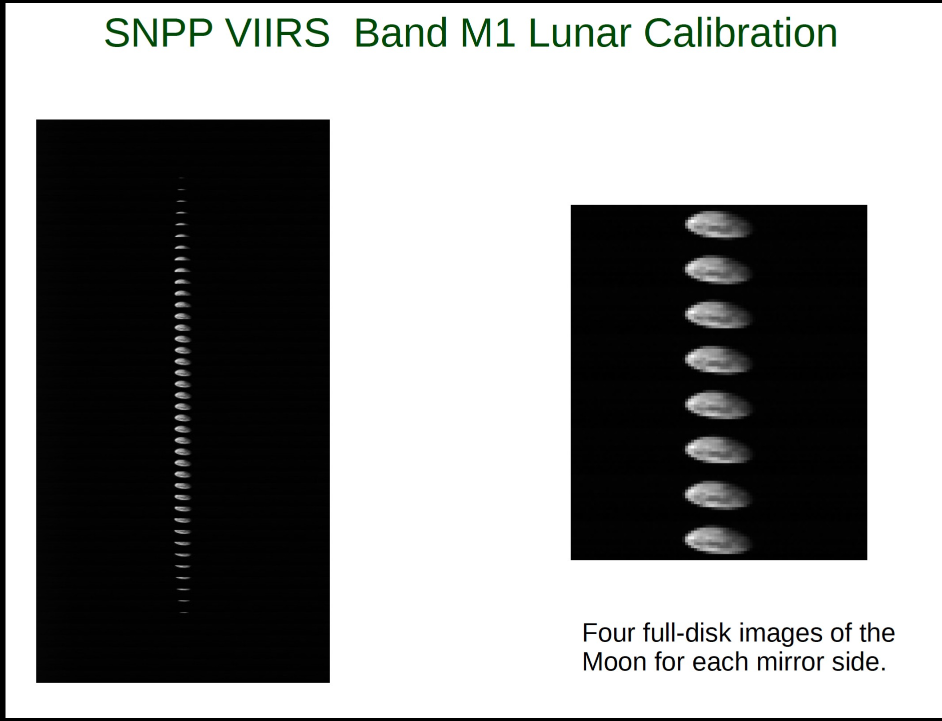


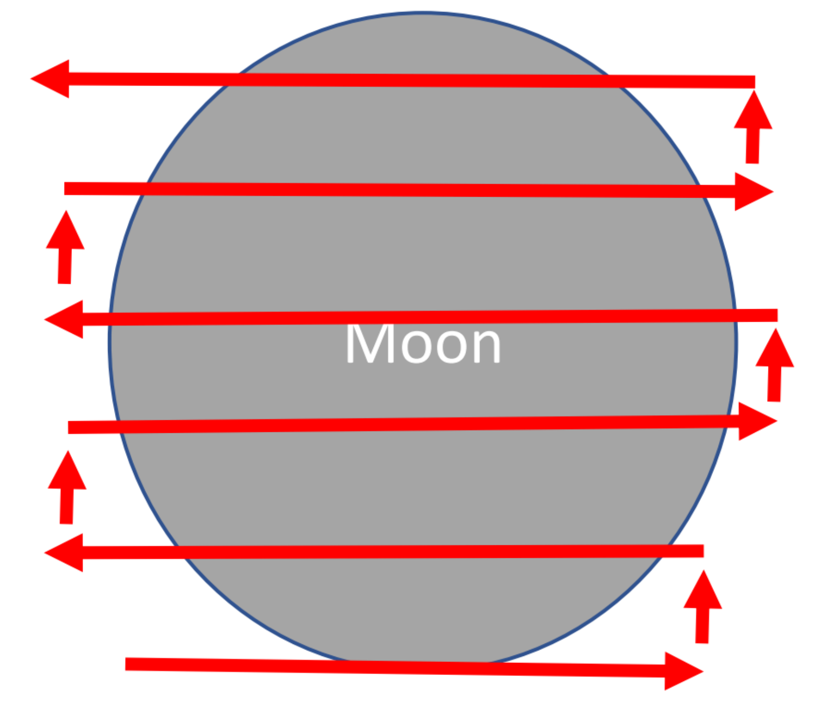


Figure 9.1. Sequence of Raster Maneuvers

# SNPP VIIRS Lunar Time Series

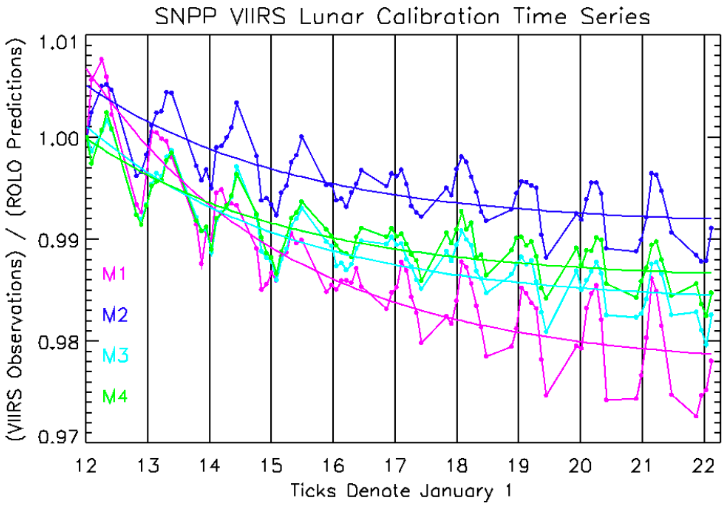


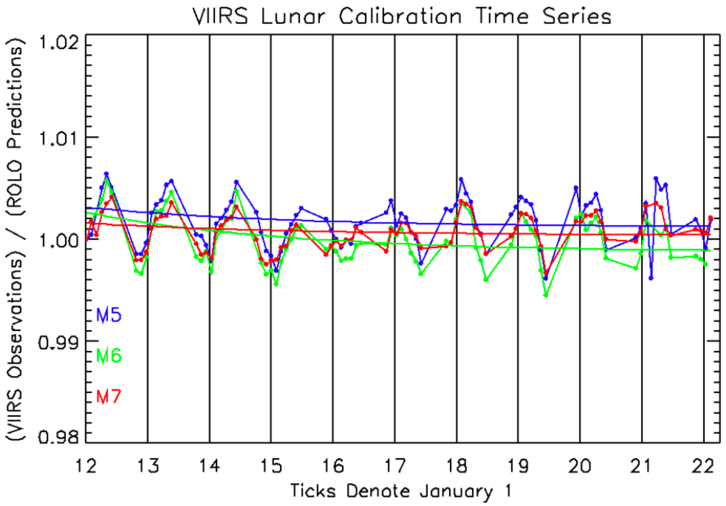


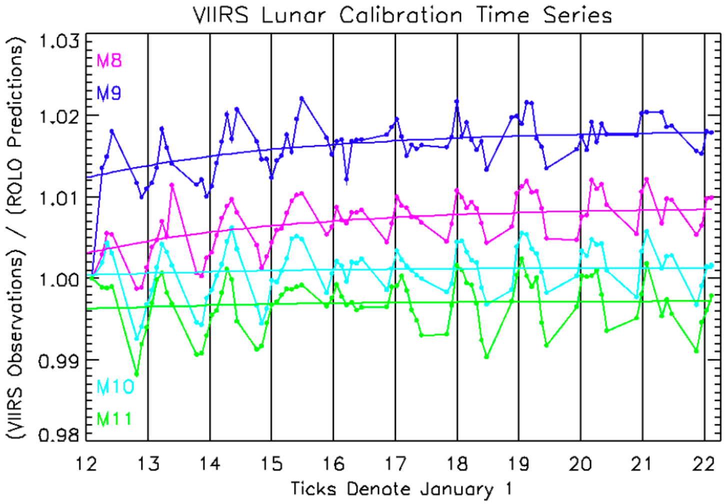

# OCI on-orbit temporal calibration plan

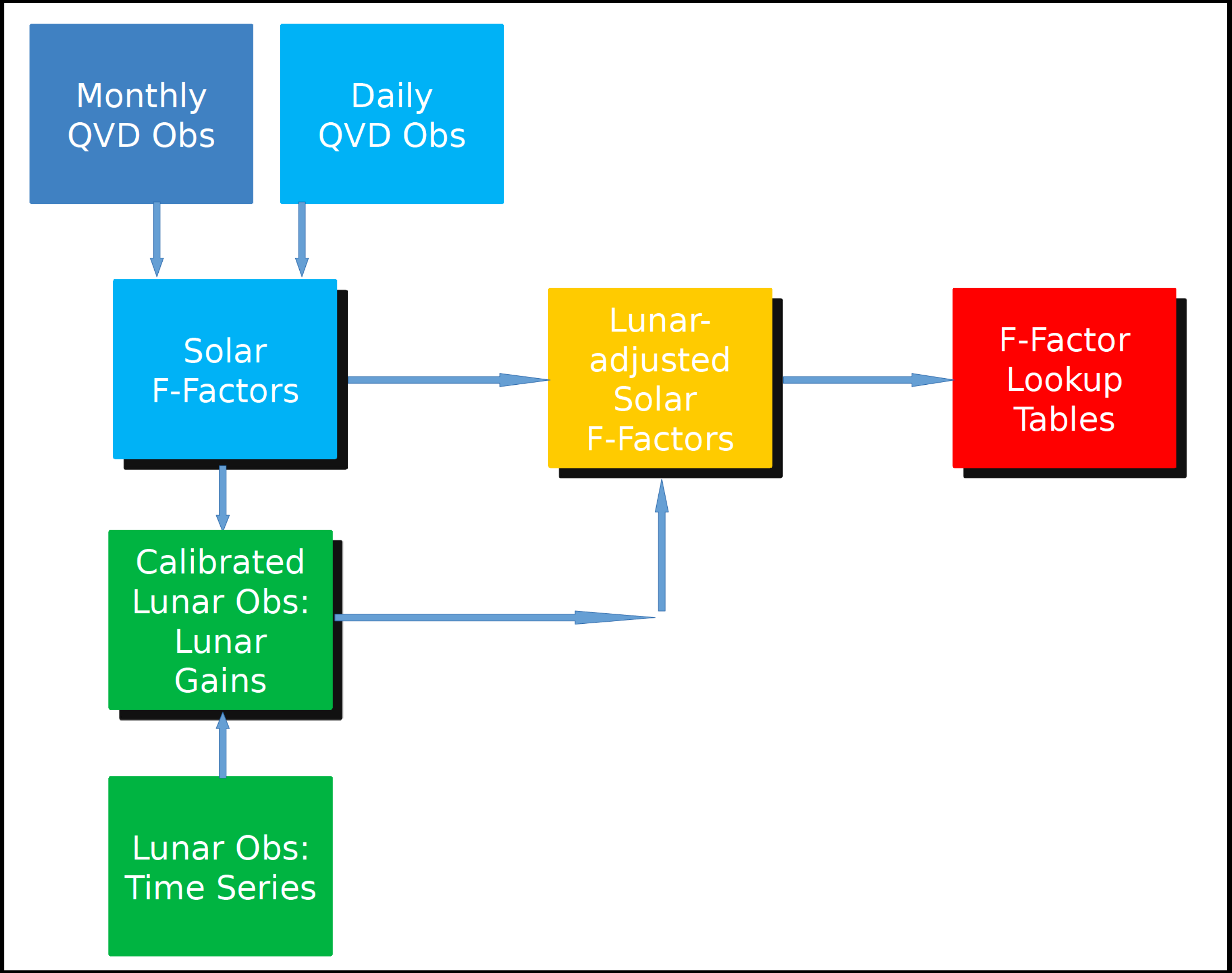

# system vicarious calibration

absolute calibration that accounts for instrument systematic biases + atmospheric correction

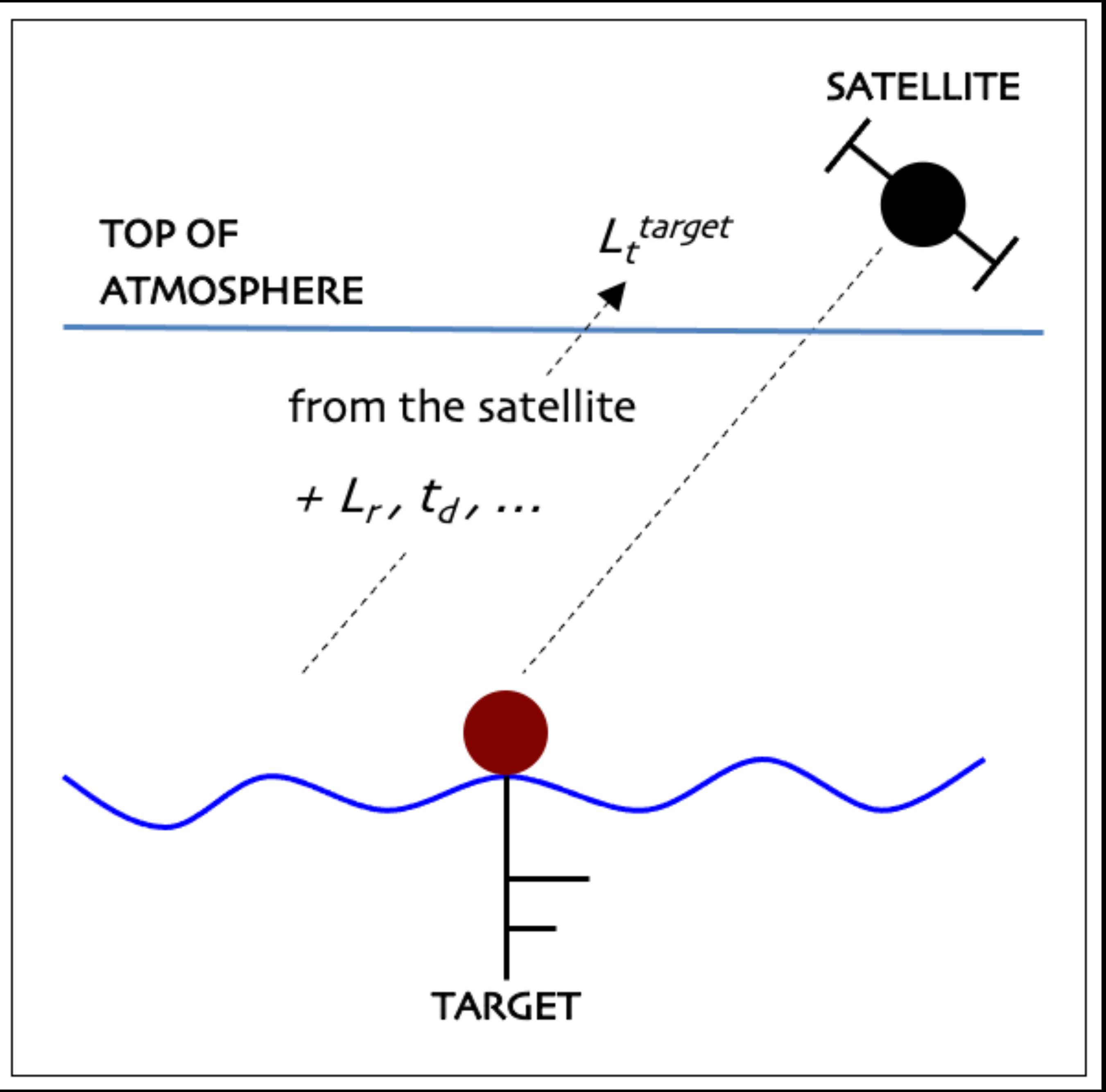

# Sensor-independent approach to the vicarious calibration of satellite ocean color radiometry

Bryan A. Franz,[1,2,*] Sean W. Bailey,[1,3] P. Jeremy Werdell,[1,4] and Charles R. McClain[1,5]

[1]Ocean Biology Processing Group, 614.8, NASA Goddard Space Flight Center, Greenbelt, Maryland 20771, USA
[2]Science Applications International Corporation, 10260 Campus Point Dr., San Diego, California 92121, USA
[3]Futuretech Corp., 7307 Hanover Pkwy., Suite D, Greenbelt, Maryland 20770, USA
[4]Science Systems and Applications, Inc., 10210 Greenbelt Rd., Suite 600, Lanham, Maryland 20706, USA
[5]National Aeronautics and Space Administration, 614.8, NASA Goddard Space Flight Center, Greenbelt, Maryland 20771, USA

*Corresponding author: bryan.franz@gsfc.nasa.gov

Received 5 February 2007; revised 2 April 2007; accepted 3 April 2007;
posted 4 April 2007 (Doc. ID 79697); published 9 July 2007

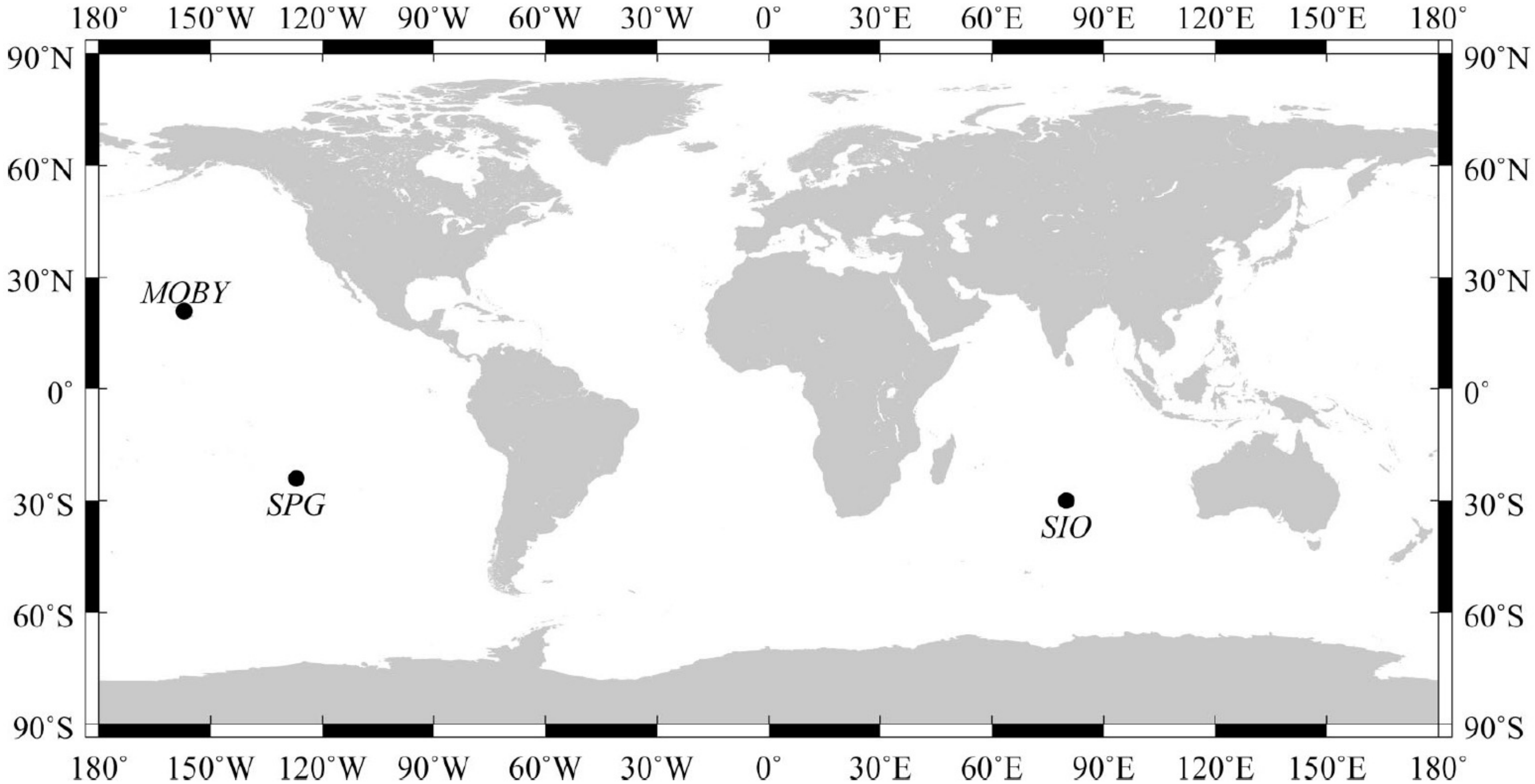


Fig. 2. Map showing location of the vicarious calibration sites used operationally by the OBPG for the calibration of SeaWiFS and other ocean color sensors. The MOBY site is used for the calibration of the visible wavelengths. The locations in the SPG and SIO are used for the vicarious calibration of the NIR wavelength(s).

# NIR vicarious calibration

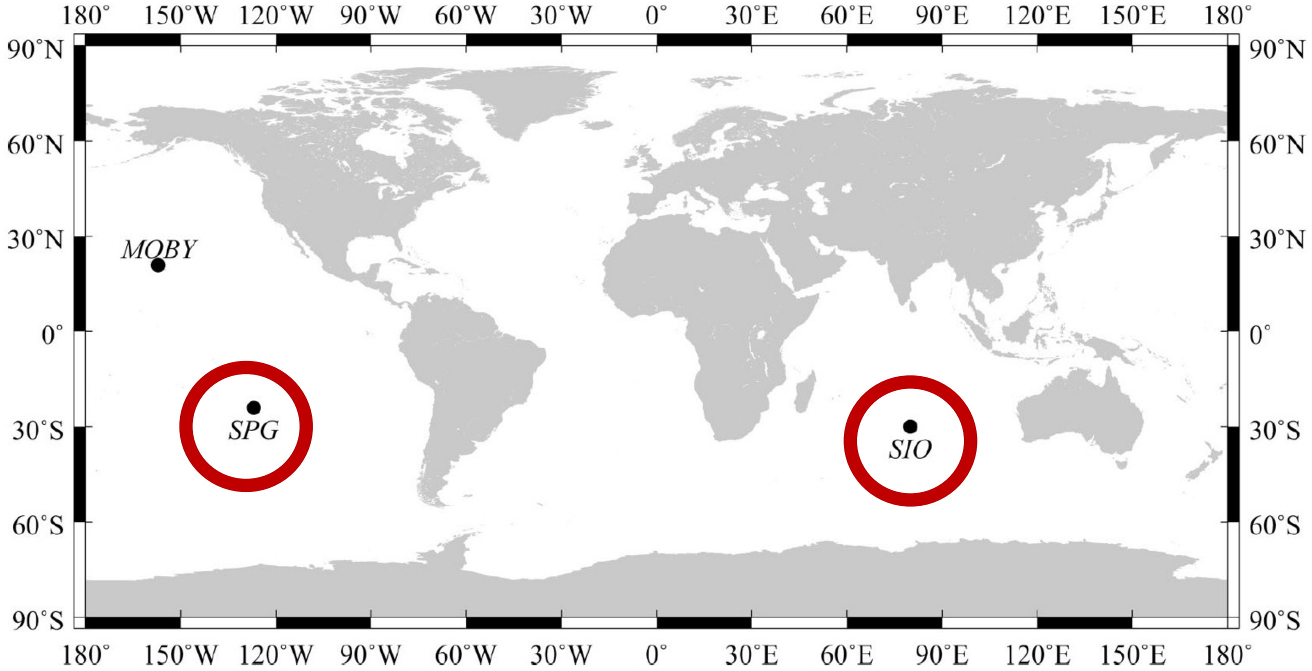


Fig. 2. Map showing location of the vicarious calibration sites used operationally by the OBPG for the calibration of SeaWiFS and other ocean color sensors. The MOBY site is used for the calibration of the visible wavelengths. The locations in the SPG and SIO are used for the vicarious calibration of the NIR wavelength(s).

assume long wavelength (865 nm for SeaWiFS) gain = 1.0

assume known aerosol properties

calculate gain for short wavelength (765 nm for SeaWiFS) assuming Rrs = 0 $sr^{-1}$)

# visible vicarious calibration

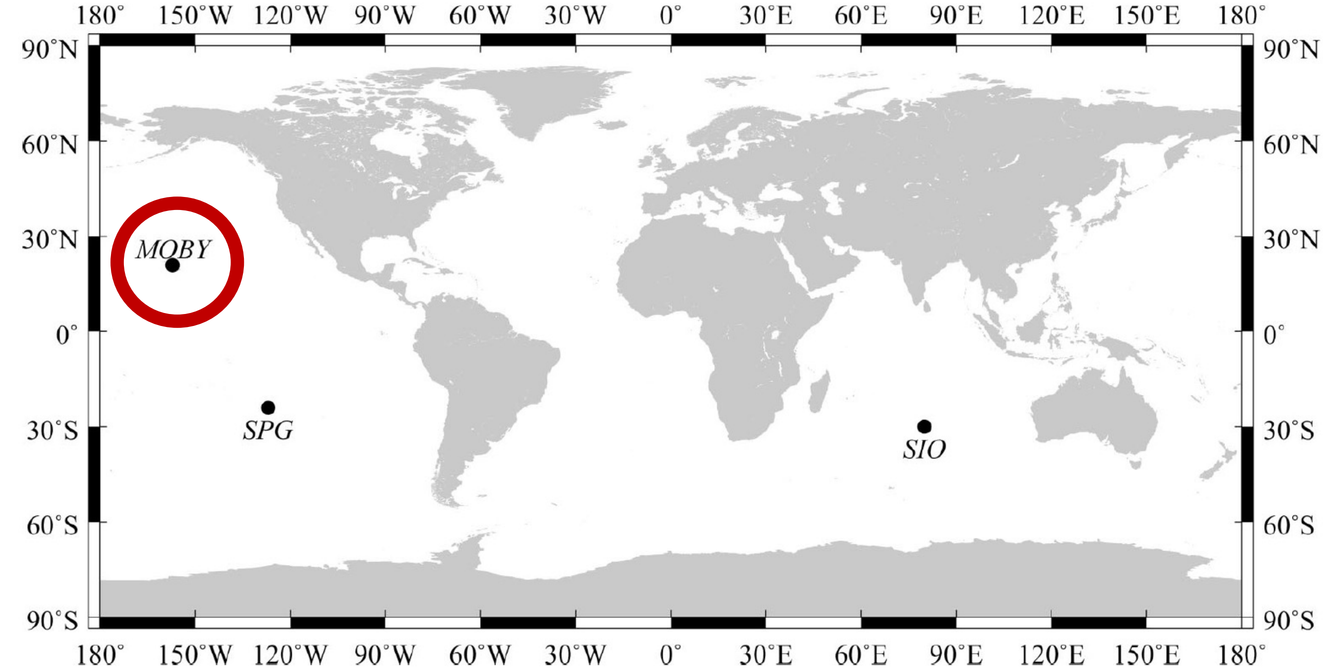


Fig. 2. Map showing location of the vicarious calibration sites used operationally by the OBPG for the calibration of SeaWiFS and other ocean color sensors. The MOBY site is used for the calibration of the visible wavelengths. The locations in the SPG and SIO are used for the vicarious calibration of the NIR wavelength(s).

performed after NIR vicarious calibration

requires ”truth” measurement at wavelengths of interest

# MOBY - the Marine Optical BuoY

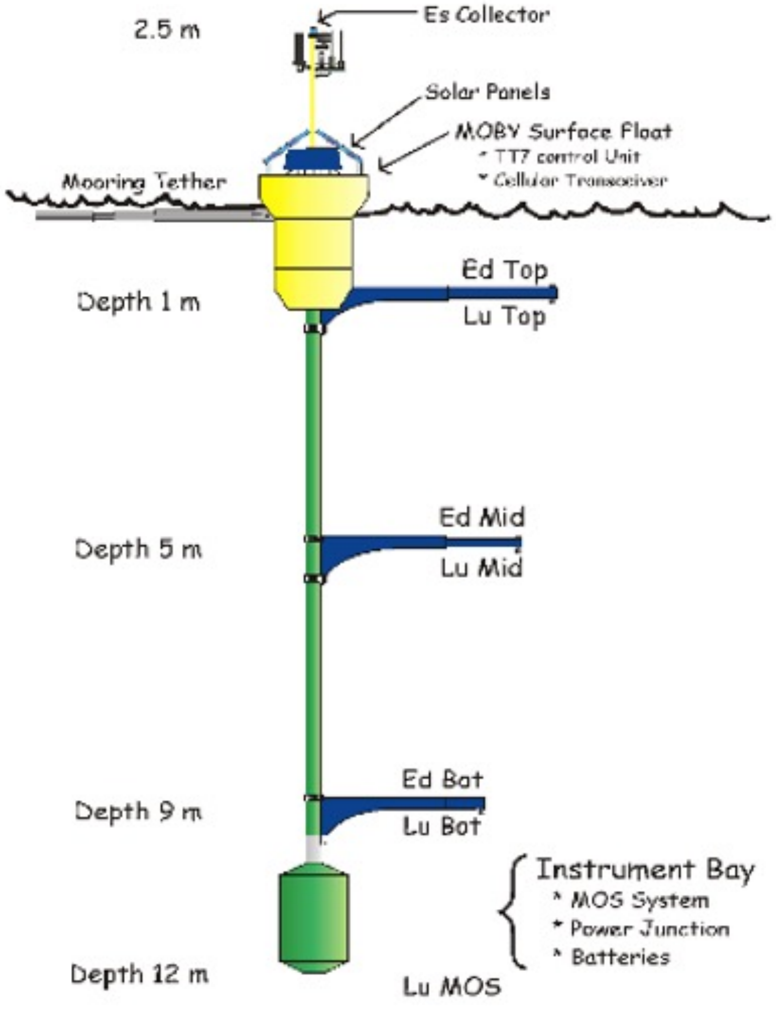


Fig. 1. Schematic diagram of MOBY.

maintained by UMiami, NOAA, NIST, & Moss Landing Marine Laboratory

20 miles west of Lanai, Hawaii

$L_u(\lambda)$ and $E_d(\lambda)$ at nominal depths of 1, 5, and 9 meters, plus $E_s(\lambda)$

spectral range is 340-955 nm & spectral resolution is 0.6 nm

hyperspectral data convolved to specific bandpasses of each satellite

# ~40 match-ups required to achieve "stable" vicarious gain

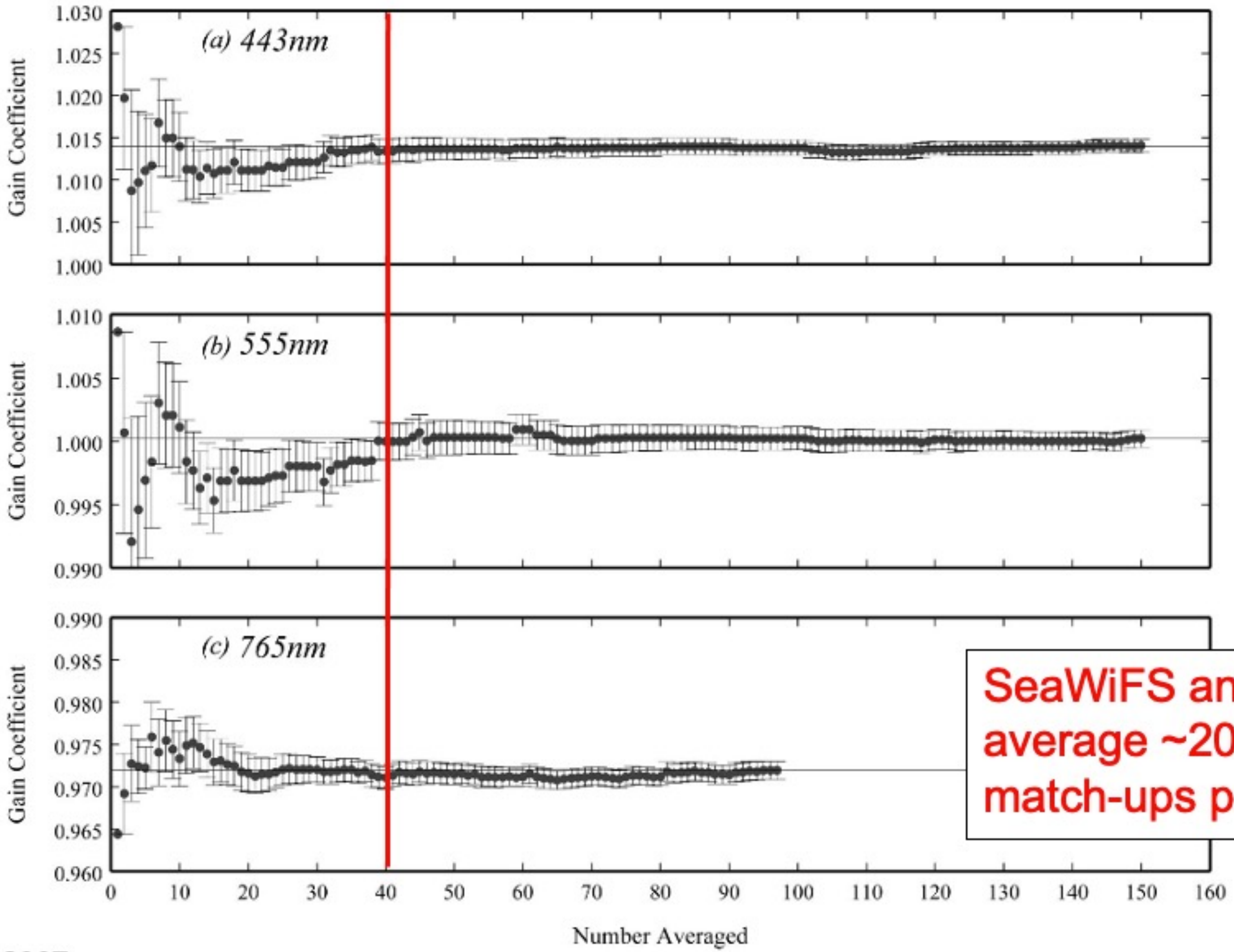


SeaWiFS and Aqua average ~20 MOBY match-ups per year

# a single, spectral radiometric adjustment

gain vs. time

gain vs. solar zenith angle

gain vs. satellite zenith angle

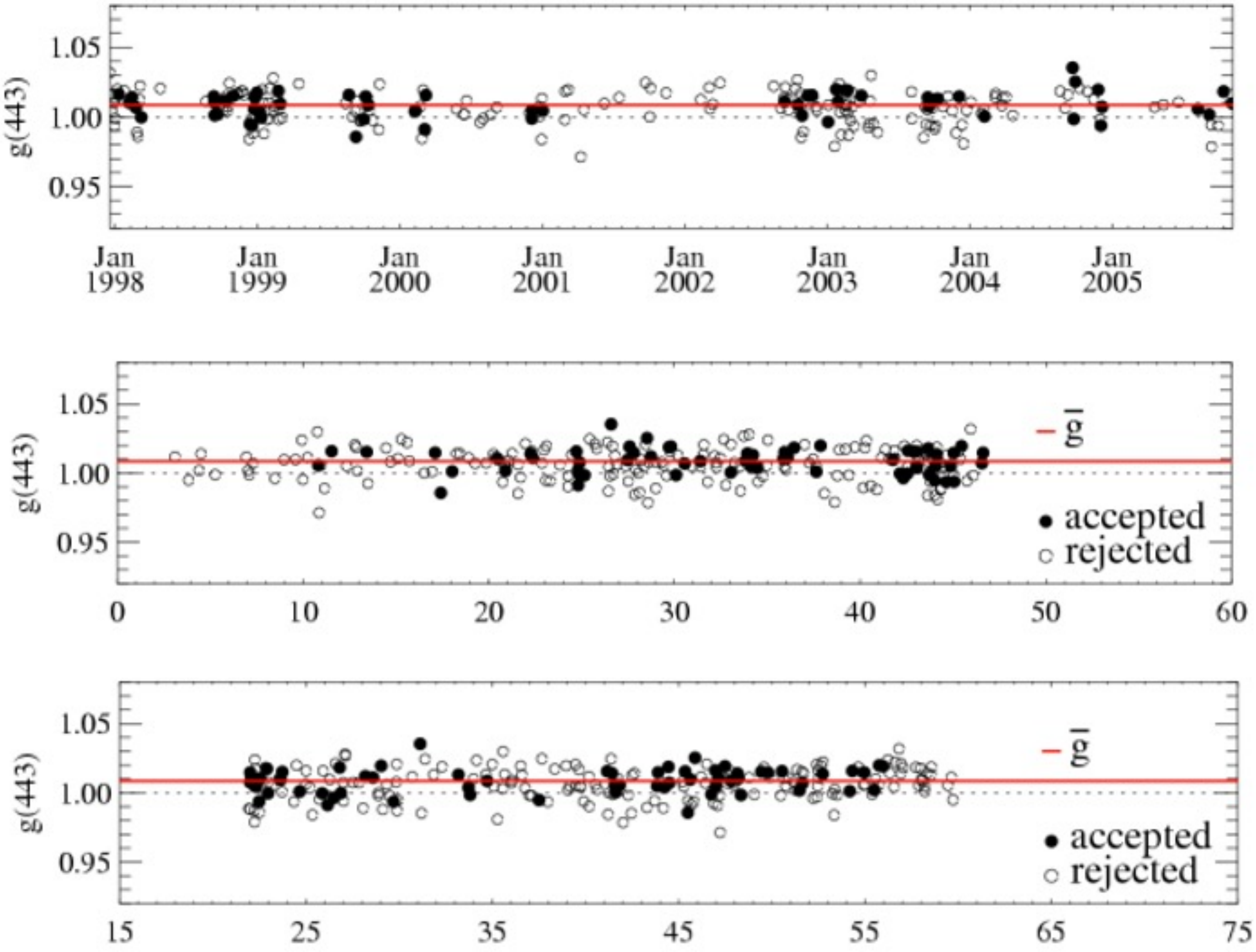

**Table 2. SeaWiFS Vicarious Gain Coefficients**

| $\lambda$ | 412 | 443 | 490 | 510 | 555 | 670 | 765 | 865 | N[a] |
|---|---|---|---|---|---|---|---|---|---|
| $\bar{g}$ | 1.0377 | 1.014 | 0.9927 | 0.9993 | 1.000 | 0.9738 | 0.9720 | 1.000 | 150 (97) |
| $\sigma$[b] | 0.009 | 0.009 | 0.008 | 0.009 | 0.008 | 0.007 | 0.010 | 0.0 | |
| $S_E$[c] | 0.0007 | 0.0007 | 0.0007 | 0.0007 | 0.0007 | 0.0006 | 0.0011 | 0.0 | |

[a]Number of gain samples, $g_i$, used to compute the mean gain, $\bar{g}$, for $\lambda < 765$ ($\lambda = 765$).
[b]Standard deviation of the distribution of $g_i$ about $\bar{g}$.
[c]Standard error on the mean, $\bar{g}$, computed as $\sigma$/sqrt(N).

**Table 4. Validation of Vicarious Calibration Against Deep-Water *In Situ* Measurements**

| | Ratio[a] | MPD[a] | $r^2$ | N[b] |
|---|---|---|---|---|
| $L_{wn}(412)$ | 1.002 | 11.8 | 0.930 | 188 |
| $L_{wn}(443)$ | 0.950 | 15.5 | 0.873 | 318 |
| $L_{wn}(490)$ | 0.942 | 12.2 | 0.817 | 318 |
| $L_{wn}(510)$ | 0.957 | 10.6 | 0.579 | 164 |
| $L_{wn}(555)$ | 0.968 | 14.8 | 0.827 | 318 |
| $L_{wn}(670)$ | 1.347 | 64.7 | 0.595 | 306 |
| $C_a$ | 0.994 | 26.1 | 0.875 | 149 |

[a]As defined in Table 3.
[b]Number of satellite to *in situ* match-up cases.

**Table 6. Sensitivity of Deep-Water Validation to NIR only Calibration; $\bar{g}(765) = 0.9720$**

| $\bar{g}(\lambda)$ | Ratio[a] | MPD[a] | $r^2$ | $N^b$ |
|---|---|---|---|---|
| 1.0000 | 0.595 | 40.6 | 0.915 | 188 |
| 1.0000 | 0.779 | 23.5 | 0.866 | 318 |
| 1.0000 | 1.002 | 11.3 | 0.816 | 318 |
| 1.0000 | 0.964 | 10.7 | 0.571 | 164 |
| 1.0000 | 0.965 | 15.0 | 0.822 | 318 |
| 1.0000 | 3.565 | 256.0 | 0.572 | 306 |

**Table 4. Validation of Vicarious Calibration Against Deep-Water *In Situ* Measurements**

| | Ratio[a] | MPD[a] | $r^2$ | N[b] |
|---|---|---|---|---|
| $L_{wn}(412)$ | 1.002 | 11.8 | 0.930 | 188 |
| $L_{wn}(443)$ | 0.950 | 15.5 | 0.873 | 318 |
| $L_{wn}(490)$ | 0.942 | 12.2 | 0.817 | 318 |
| $L_{wn}(510)$ | 0.957 | 10.6 | 0.579 | 164 |
| $L_{wn}(555)$ | 0.968 | 14.8 | 0.827 | 318 |
| $L_{wn}(670)$ | 1.347 | 64.7 | 0.595 | 306 |
| $C_a$ | 0.994 | 26.1 | 0.875 | 149 |

[a]As defined in Table 3.
[b]Number of satellite to *in situ* match-up cases.

**Table 9. Sensitivity of Deep-Water Validation to M50 765-nm Calibration; $\bar{g}(765) = 0.9835$**

| | $\bar{g}(\lambda)$ | Ratio[a] | MPD[a] | $r^2$ | $N$[b] |
|---|---|---|---|---|---|
| $L_{wn}(412)$ | 1.0467 | 0.995 | 10.8 | 0.931 | 188 |
| $L_{wn}(443)$ | 1.0245 | 0.955 | 16.0 | 0.879 | 318 |
| $L_{wn}(490)$ | 1.0050 | 0.934 | 13.4 | 0.826 | 318 |
| $L_{wn}(510)$ | 1.0131 | 0.953 | 10.6 | 0.608 | 164 |
| $L_{wn}(555)$ | 1.0164 | 0.961 | 14.3 | 0.844 | 318 |
| $L_{wn}(670)$ | 0.9915 | 1.399 | 53.5 | 0.599 | 306 |
| $C_a$ | | 1.007 | 26.0 | 0.871 | 149 |

[a]As defined in Table 3.
[b]Number of satellite-to-*in situ* match-up cases (a common set was used for Tables 6–10 and for the analysis presented in Table 4).

**Table 10. Sensitivity of Deep-Water Validation to O99 765-nm Calibration; $\bar{g}(765) = 0.9594$**

| $\bar{g}(\lambda)$ | Ratio[a] | MPD[a] | $r^2$ | $N$[b] |
|---|---|---|---|---|
| 1.0285 | 0.999 | 12.1 | 0.925 | 188 |
| 1.0031 | 0.957 | 14.2 | 0.866 | 318 |
| 0.9793 | 0.947 | 12.2 | 0.804 | 318 |
| 0.9840 | 0.968 | 10.6 | 0.559 | 164 |
| 0.9825 | 0.967 | 14.9 | 0.805 | 318 |
| 0.9544 | 1.341 | 63.8 | 0.594 | 306 |
| | 0.943 | 25.5 | 0.872 | 149 |

[a]As defined in Table 3.
[b]Number of satellite-to-*in situ* match-up cases (a common set was used for Tables 6–10 and for the analysis presented in Table 4).

**Table 7. Sensitivity of Deep-Water Validation to Calibration Assumptions +4% 865-nm Calibration; $\bar{g}(765) = 1.0007$**

| | $\bar{g}(\lambda)$ | Ratio[a] | MPD[a] | $r^2$ | $N$[b] |
|---|---|---|---|---|---|
| $L_{wn}(412)$ | 1.0405 | 0.998 | 11.8 | 0.927 | 188 |
| $L_{wn}(443)$ | 1.0177 | 0.953 | 14.8 | 0.871 | 318 |
| $L_{wn}(490)$ | 0.9982 | 0.944 | 12.5 | 0.812 | 318 |
| $L_{wn}(510)$ | 1.0059 | 0.965 | 10.8 | 0.573 | 164 |
| $L_{wn}(555)$ | 1.0099 | 0.977 | 15.3 | 0.822 | 318 |
| $L_{wn}(670)$ | 0.9933 | 1.416 | 61.4 | 0.596 | 306 |
| $C_a$ | | 0.980 | 26.2 | 0.873 | 149 |

[a]As defined in Table 3.
[b]Number of satellite-to-*in situ* match-up cases (a common set was used for Tables 6–10 and for the analysis presented in Table 4).

**Table 8. Sensitivity of Deep-Water Validation to −4% 865-nm Calibration; $\bar{g}(765) = 0.9420$**

| $\bar{g}(\lambda)$ | Ratio[a] | MPD[a] | $r^2$ | $N$[b] |
|---|---|---|---|---|
| 1.0337 | 1.005 | 11.0 | 0.932 | 188 |
| 1.0090 | 0.954 | 15.2 | 0.876 | 318 |
| 0.9856 | 0.940 | 12.4 | 0.822 | 318 |
| 0.9908 | 0.953 | 11.2 | 0.591 | 164 |
| 0.9885 | 0.958 | 14.0 | 0.837 | 318 |
| 0.9527 | 1.376 | 57.0 | 0.604 | 306 |
| | 0.987 | 24.7 | 0.875 | 149 |

[a]As defined in Table 3.
[b]Number of satellite-to-*in situ* match-up cases (a common set was used for Tables 6–10 and for the analysis presented in Table 4).

# alternative sources of “truth”

**On-orbit vicarious calibration of ocean color sensors using an ocean surface reflectance model**

10 August 2007 / Vol. 46, No. 23 / APPLIED OPTICS 5649

P. Jeremy Werdell,[1,*] Sean W. Bailey,[1] Bryan A. Franz,[1] André Morel,[2] and Charles R. McClain[1]

**Sources and assumptions for the vicarious calibration of ocean color satellite observations**

Sean W. Bailey,[1,2,*] Stanford B. Hooker,[3] David Antoine,[4]
Bryan A. Franz,[1,5] and P. Jeremy Werdell[1,6]

20 April 2008 / Vol. 47, No. 12 / APPLIED OPTICS 2035

build a climatology using a long-term Chl record (this is for BATS, near Bermuda) …

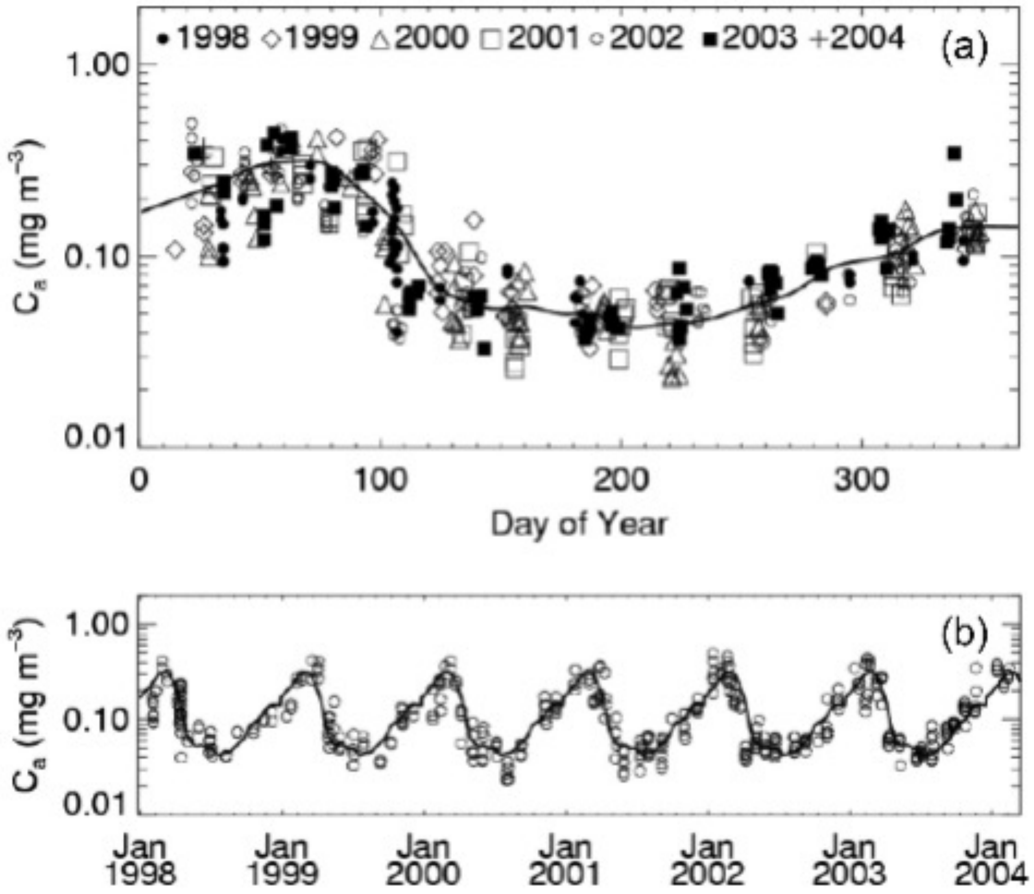


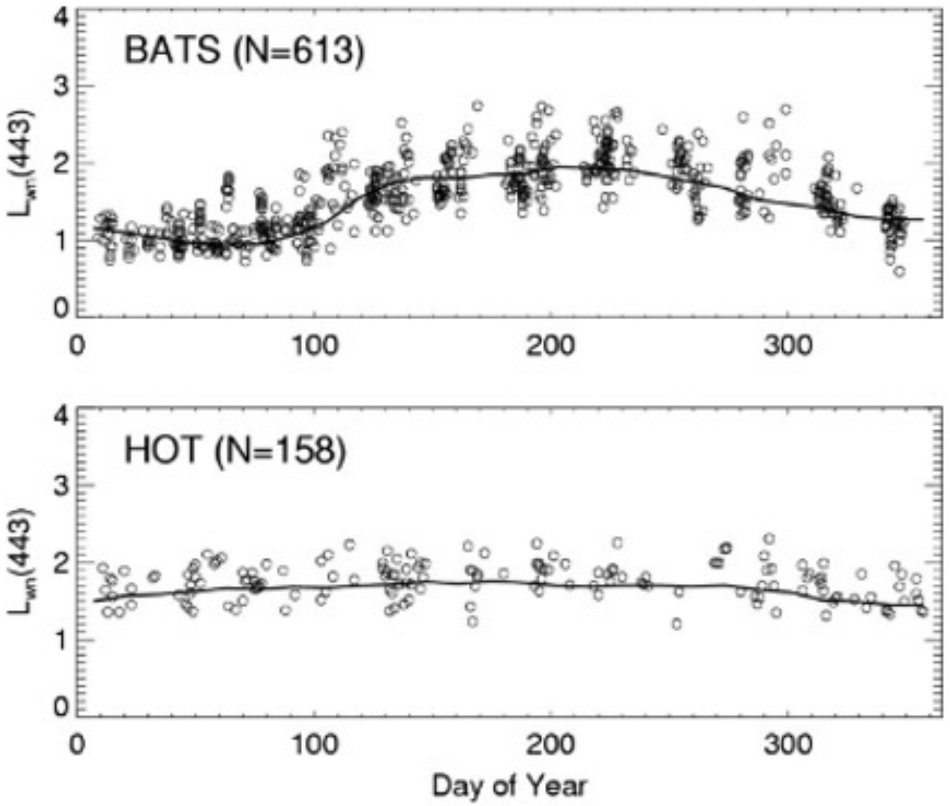


$$L_{wn}(\lambda) = F(\mathrm{Chl})$$

… then, develop a $L_{wn}(\lambda)$ or $R_{rs}(\lambda)$ climatology using an ocean reflectance model (e.g., Morel & Maritorena 2001)

Table 3. Percent Differences[a] Between the MOBY and ORM $\bar{g}$

| | 412 | 443 | 490 | 510 | 555 | 670 |
|---|---|---|---|---|---|---|
| BATS | −0.31 | −1.18 | −1.14 | −0.52 | 0.14 | −0.07 |
| HOTS | −0.74 | −0.53 | −0.48 | −0.14 | 0.44 | −0.21 |
| BATS + HOTS | −0.52 | −0.86 | −0.81 | −0.33 | 0.29 | −0.13 |

[a]Calculated using $(\bar{g}_{\mathrm{ORM}} - \bar{g}_{\mathrm{MOBY}}) \times 100\%/\bar{g}_{\mathrm{MOBY}}$.

model-based gains typically differ from MOBY gains by < 1%

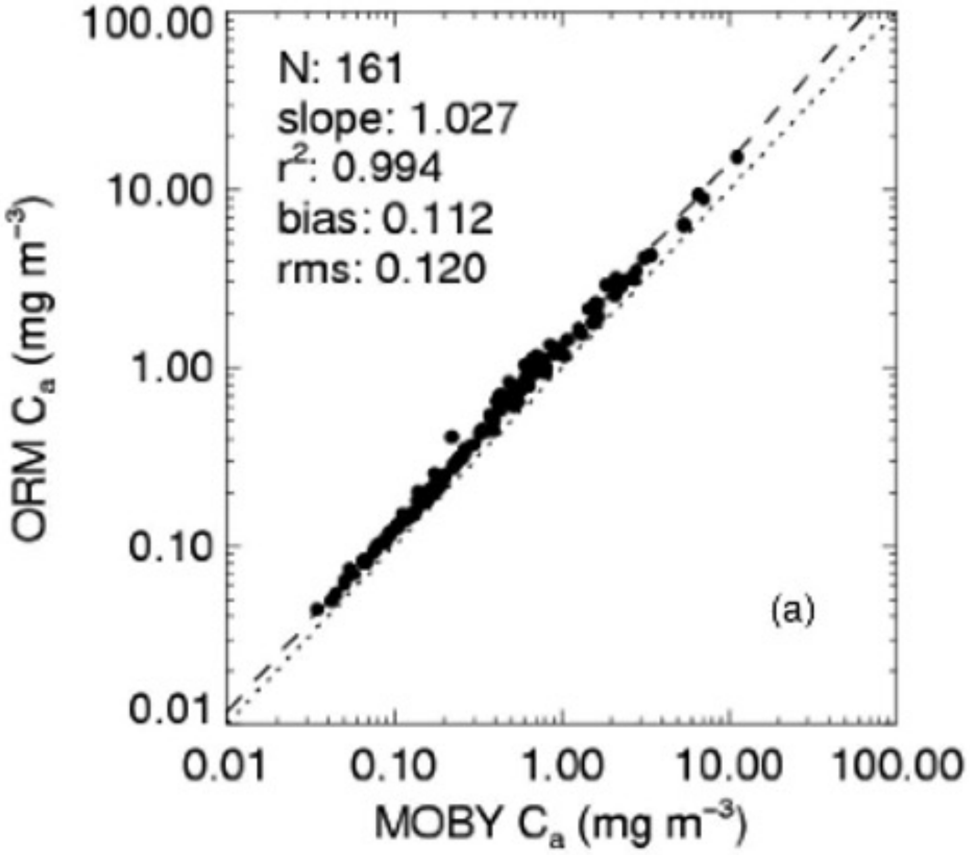

AERONET (fixed-above water platforms)

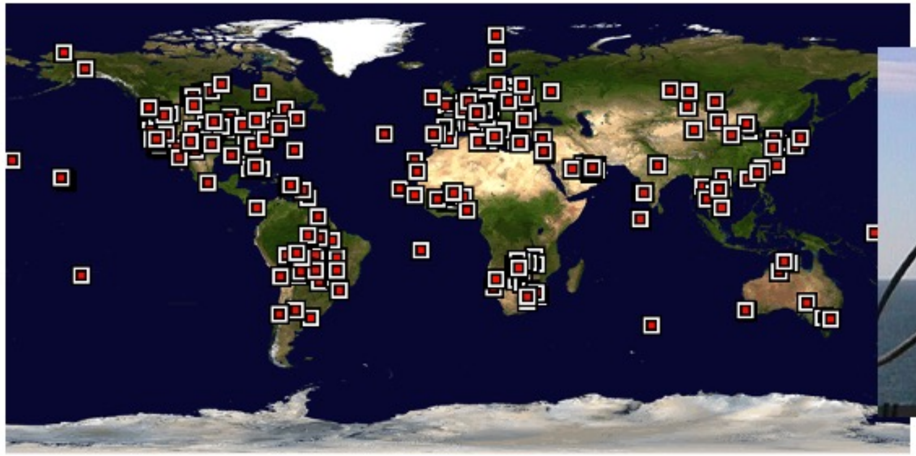

buoy networks

gliders, drifters, & other autonomous platforms

towed & underway sampling

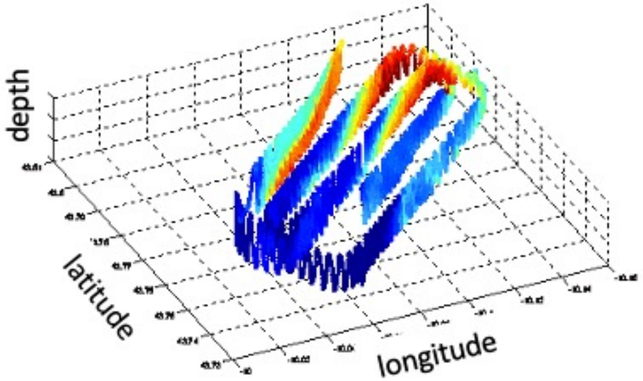

gains calculated using alternative *in situ* data typically differ from MOBY by < 0.3%

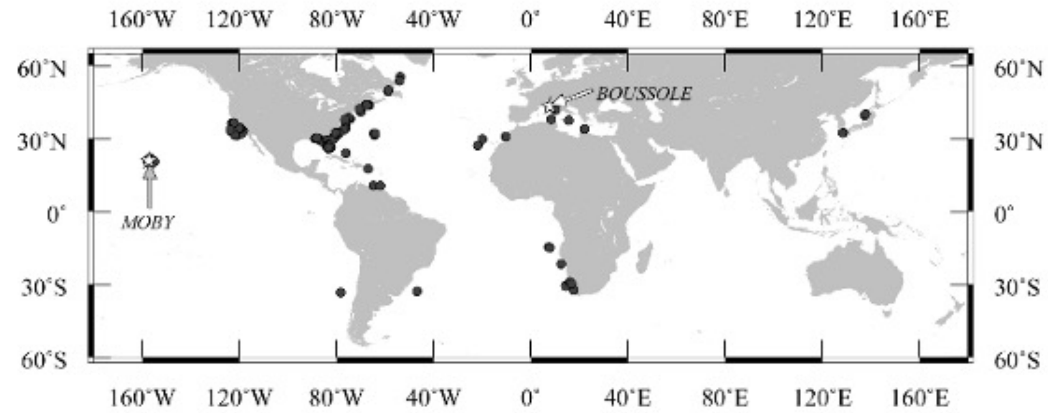


Fig. 1. Map showing the locations for the *in situ* data used in this study.

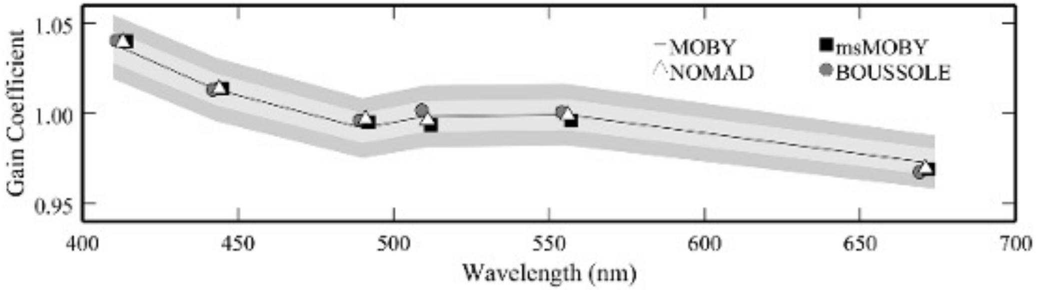


Fig. 3. Vicarious calibration coefficients as a function of wavelength. The standard MOBY-derived $\bar{g}_{\lambda}'$ (solid curve) are overplotted by the msMOBY-, NOMAD-, and BOUSSOLE-derived $\bar{g}_{\lambda}'$. The shaded regions indicate the ranges for the first (light-gray) and second (dark-gray) standard deviations of the mean for $\bar{g}_{\lambda}'$.

Bailey et al. 2008

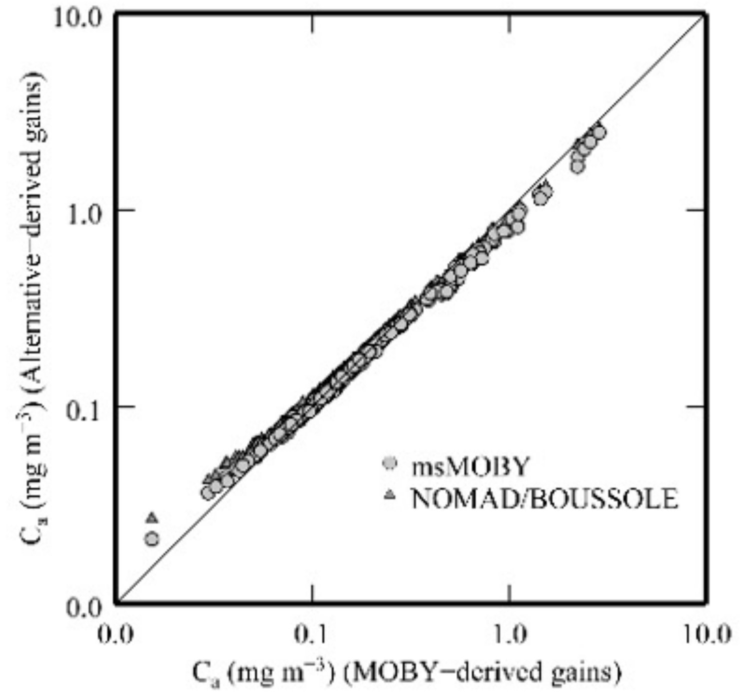


Fig. 7. Satellite-derived chlorophyll estimated from the two alternative $\bar{g}'$ gain sets (msMOBY and NOMAD/BOUSSOLE) plotted versus the corresponding chlorophyll estimated from the standard MOBY $\bar{g}$.

the gains shown previously for the multiple "ground-truth" targets differ only from 0.3 to 1%, but there are spectral dependencies in their differences …

spectral differences impart **changes** in derived products looking forward

Remote Sensing of Environment 260 (2021) 112439

ELSEVIER

Contents lists available at ScienceDirect

Remote Sensing of Environment

journal homepage: www.elsevier.com/locate/rse

Check for updates

# Cross-calibration of MODIS and VIIRS long near infrared bands for ocean color science and applications

Brian B. Barnes [a,*], Chuanmin Hu [a], Sean W. Bailey [b], Nima Pahlevan [b,c], Bryan A. Franz [b]

[a] College of Marine Science, University of South Florida, St. Petersburg, FL 33701, USA
[b] NASA Goddard Space Flight Center, 8800 Greenbelt Road, Greenbelt, MD 20771, USA
[c] Science Systems and Applications Inc., 10210 Greenbelt Road, Lanham, MD 20706, USA



# Sensitivity of Satellite Ocean Color Data to System Vicarious Calibration of the Long Near Infrared Band

Brian B. Barnes, Chuanmin Hu, Sean W. Bailey, and Bryan A. Franz

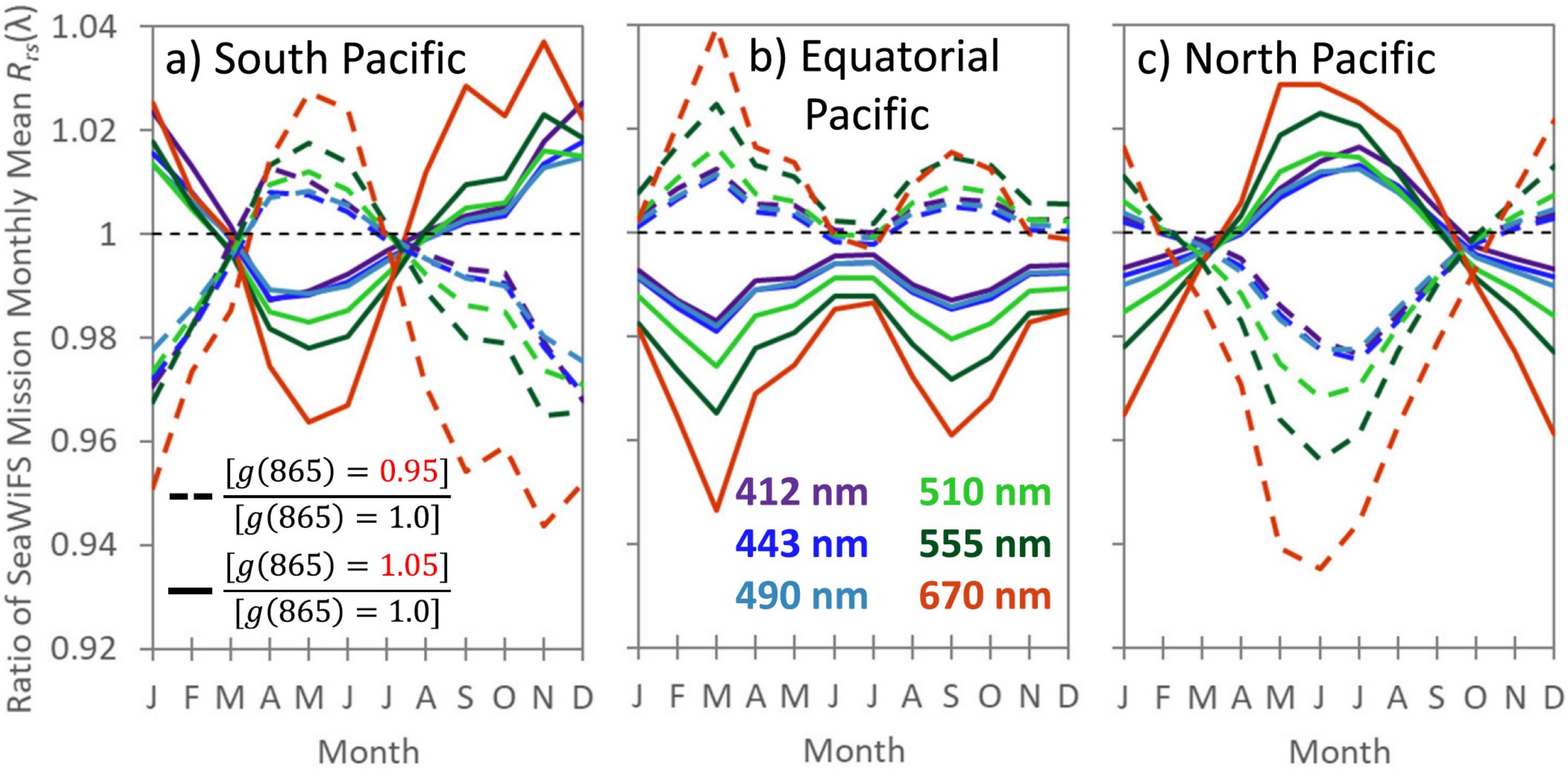

Ratio of SeaWiFS Mission Monthly Mean $R_{rs}(\lambda)$
1.04
1.02
1
0.98
0.96
0.94
0.92
a) South Pacific
b) Equatorial Pacific
c) North Pacific
$\frac{[g(865) = 0.95]}{[g(865) = 1.0]}$
$\frac{[g(865) = 1.05]}{[g(865) = 1.0]}$
412 nm
443 nm
490 nm
510 nm
555 nm
670 nm
J F M A M J J A S O N D
Month

# Adjustment of ocean color sensor calibration through multi-band statistics

**Richard P. Stumpf [1*] and P. Jeremy Werdell [2]**

[1] *NOAA National Ocean Service, 1305 East–west Highway N/SCI1, Silver Spring, Maryland 20910, USA*
[2] *Science Systems and Applications, Inc., NASA Goddard Space Flight Center, Greenbelt, Maryland 20771, USA*
* *richard.stumpf@noaa.gov*

#114396 - $15.00 USD Received 16 Jul 2009; revised 13 Nov 2009; accepted 1 Dec 2009; published 4 Jan 2010

18 January 2010 / Vol. 18, No. 2 / OPTICS EXPRESS 401

## population statistics for vicarious calibration

compare spectral shapes of *in situ* & satellite populations

$$SS(\lambda) = R_{rs}(\lambda) - R_{rs}(\lambda^-) - \left[R_{rs}(\lambda^+) - R_{rs}(\lambda^-)\right]\left(\frac{\lambda - \lambda^-}{\lambda^+ - \lambda^-}\right)$$

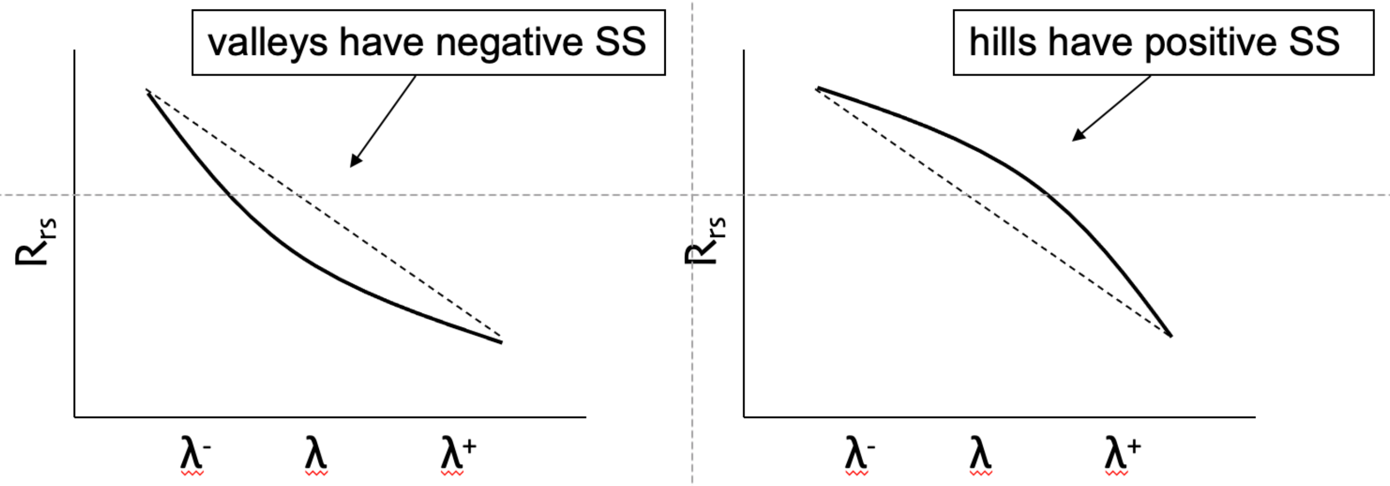


spectral shape @ 443 nm, SS(443), uses $R_{rs}(412)$, $R_{rs}(443)$, & $R_{rs}(490)$

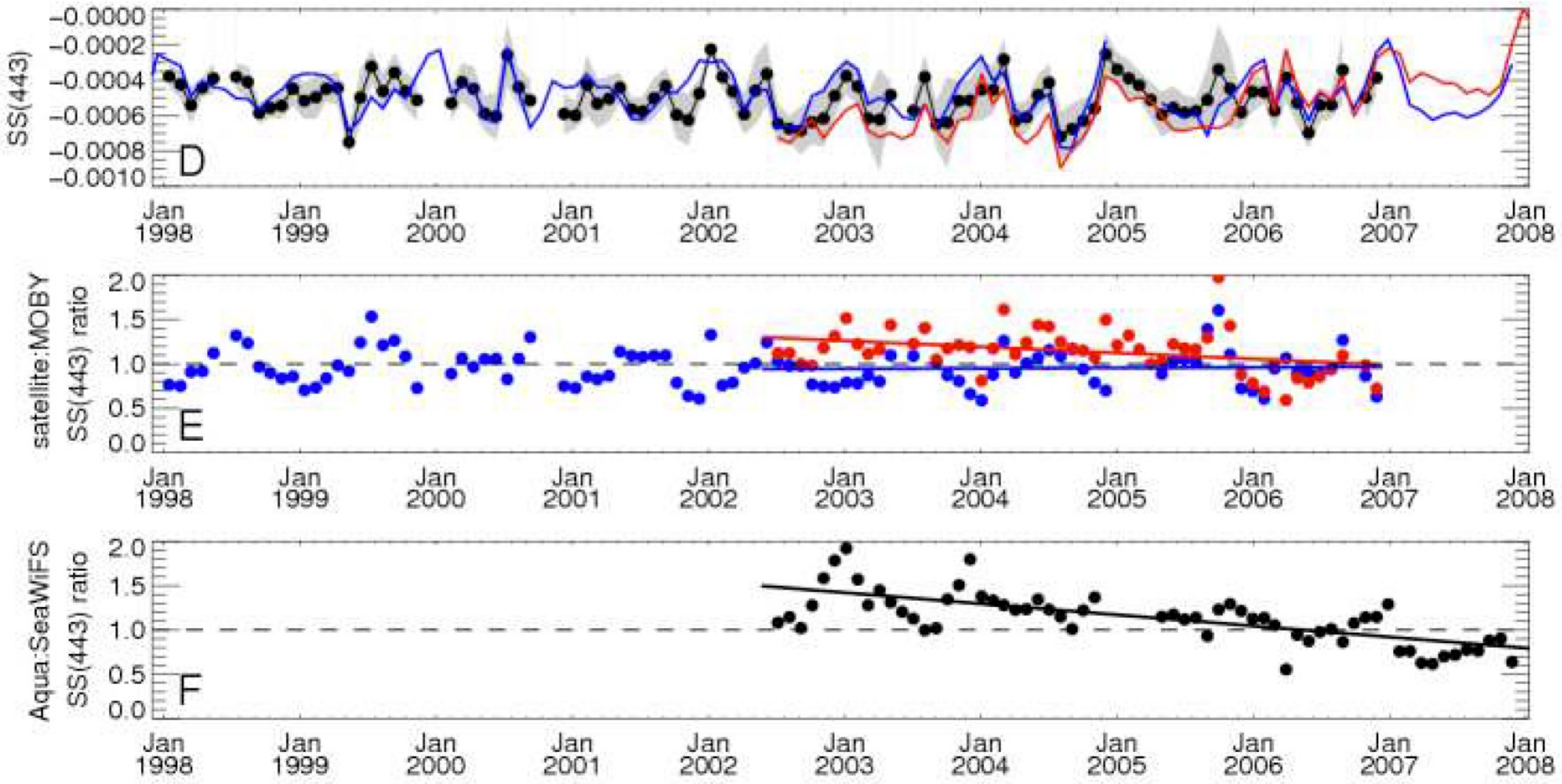

SS(443)
-0.0000
-0.0002
-0.0004
-0.0006
-0.0008
-0.0010
D
satellite:MOBY
SS(443) ratio
E
Aqua:SeaWiFS
SS(443) ratio
F
0.0
0.5
1.0
1.5
2.0
Jan 1998
Jan 1999
Jan 2000
Jan 2001
Jan 2002
Jan 2003
Jan 2004
Jan 2005
Jan 2006
Jan 2007
Jan 2008

# System Vicarious Calibration (SVC)

*use of "truth" measurements to calculate another spectral absolute calibration once on orbit*

(1) HyperNAV

SeaBird Scientific

radiometric float
- small
- portable
- profiling
- long-duration
- COTS legacies

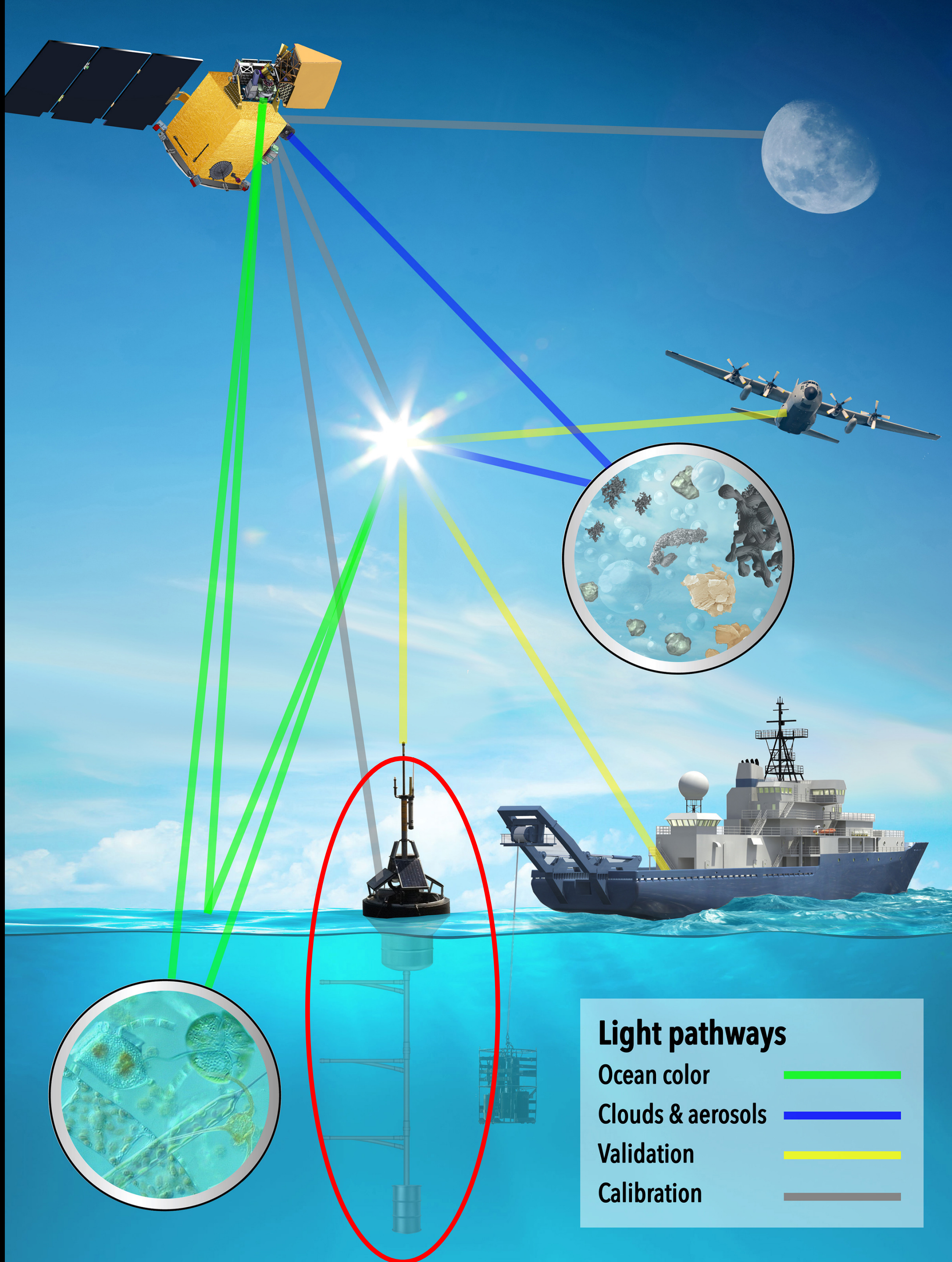

# System Vicarious Calibration (SVC)

*system requirements: hyperspectral UV-NIR, temporal stability, NIST-traceable, NRT data distribution ( O[days] )*

(2) MarONet

U.Miami, NIST

radiometric buoy
- large
- 20’ container
- 3 fixed arms
- long-deployment
- MOBY legacy